Fabrication and Luminescence Characterization of Ge Wires with Uniaxial Tensile Strains Applied using Internal Stresses in Deposited Metal Thin Films

Takayoshi Shimura[1*], Shogo Tanaka[1], Takuji Hosoi[2], and Heiji Watanabe[1]

[1]*Graduate School of Engineering, Osaka University, 2-1 Yamadaoka, Suita, Osaka 565-0871, Japan*

[2]*School of Engineering, Kwansei Gakuin University, Sanda, Hyogo, Japan*

E-mail: shimura@prec.eng.osaka-u.ac.jp

We examined the fabrication process of uniaxial tensile-strained Ge wires in micro-bridge structures by utilizing the internal stresses in deposited metal thin films. This method enables strain control by adjusting film-deposition conditions, which is advantageous over previous methods that utilize internal stresses unintentionally applied to Ge-on-insulator substrates. We evaluated the internal stresses in W films formed by sputtering deposition methods. Tensile and compressive stresses were determined based on the Ar gas pressure during the deposition process. We applied tensile strain to Ge wires using 100-nm-thick W films, each with a tensile stress of 890 MPa, deposited in 1.5 Pa Ar gas. We confirmed that strains of up to 1.62% can be achieved and controlled by tuning the structural parameters of the bridge structure with the Ge wires. Photoluminescence peaks shifted to lower energies with increasing strain, in good agreement with theoretical predictions. We also used strained Ge wires to fabricate light-emitting diodes that exhibited clear electroluminescence peaks indicative of band structural modulation in the Ge wires.

Keywords:

Ge, silicon photonics, tensile strain, internal stress, photoluminescence, electroluminescence

Introduction

Silicon (Si) photonic devices are optical integrated circuits on Si substrates and have been extensively studied in recent years [1–3]. However, Si has an indirect bandgap structure and is difficult to use as a light-emitting material; therefore, light sources made of group III-V elements are employed despite the expensive bonding processes involved [4]. Germanium (Ge) is in the same group IV as Si and is drawing attention as an alternative material [5–8]. Although Ge has an indirect bandgap structure similar to Si, the energy difference between the conduction band bottoms at the Γ and L points is only 136 meV. The transition to a direct-bandgap structure is possible in Ge by applying tensile strain and/or incorporating Sn atoms. Therefore, developing various methods for modulating the bandgap structure of Ge has been an active topic of study [9–24].

One promising approach to bandgap modulation involves the use of biaxial internal tensile strain in the top Ge layers of a Ge-on-insulator (GOI) substrate [9,25–27]. In this method, Ge layers with micro-bridge structures are fabricated, and the SiO_2 underlayers are removed later. Tensile strain is concentrated at the narrow Ge bridge, which generates a uniaxial tensile strain in the bridge. Theoretical calculations show that a uniaxial tensile strain of more than 4.6% in the <100> direction enables the transition into a direct-bandgap structure [28]. A GOI substrate with a biaxial tensile strain of 0.2% enables a maximum uniaxial tensile strain of 5.7%, with significant bandgap modulation and emission efficiency enhancements achieved as a result [25]. This method utilizes the internal stress unintentionally applied to the GOI substrate, which causes the strain applied to the Ge bridge to fluctuate in response to the initial internal stress, which is a disadvantage. Therefore, in this study, we propose using internal stresses in metal thin films controlled by the sputtering deposition conditions [29]. We show that tensile strain can be controlled by changing the film deposition conditions and the shape of the Ge bridge. We also evaluated the optical characteristics of the strained Ge wires and their band structure modulation.

Control of internal stress in a tungsten film

In general, thin films formed by sputtering deposition methods have internal tensile or compressive stresses that originate from structural changes related to the pressure and temperature conditions of the deposition process [30]. Because stress is proportional to the elastic energy of the material, tungsten (W) was selected as the deposition material to leverage its high internal stress. Moreover, W does not dissolve in hydrofluoric acid. We first evaluated the internal stresses in W films by measuring the warpage of 60-μm-thick Si substrates coated with 100-mm-thick W films. Warpage was measured using a scanning white light interferometer, with stress determined using Stoney's equation: $S = Eh^2/\{(1-\nu)6Rt\}$, where $E/(1-\nu)$ is the biaxial elastic constant of Si, h is the thickness of the Si, R is the radius of curvature, and t is the thickness of the W film [31]. W sputtering was carried out under the conditions listed in Table I. Tensile and compressive stresses were determined based on the Ar gas pressure during the deposition process (Figure 1). We applied tensile strain to Ge bridges using 100-nm-thick W films, each with a tensile stress of 890 MPa, deposited in 1.5 Pa Ar gas.

Fabrication and optical properties of Ge bridge structures

The Ge layer of a *p*-type GOI (100) substrate (Ge layer thickness = 200 nm; buried oxide layer thickness = 150 nm; initial strain <0.08%) was employed. Ge bridge structures consisting of wide pads and narrow wires were fabricated by photolithography and reactive ion etching (RIE) (Figure 2). W films, each with a tensile stress of 890 MPa, were deposited on the Ge layers using the previously described sputtering method. The amount of strain applied to each narrow wire was controlled by changing the pad length from 20 to 400 μm. The SiO_2 layer under the bridge was etched off with HF vapor. As a result, the W metal film attempted to shrink and uniaxial tensile strain was applied to the narrow Ge wire. The optical microscopy images of Ge bridge structures (Figure 3) show narrow Ge wires connecting the W pad and the Ge layer. The holes in the pad were introduced during the fabrication process to promote HF-vapor etching of the SiO_2 layers under the pads.

Micro-Raman spectroscopy was used to evaluate the uniaxial lattice strains in the Ge wires, which were determined from the Ge–Ge peak shift [9]. Figure 4a shows spectra of narrow Ge wires in which the Raman peak shifts to lower wavenumbers as the pad length was increased from 20 to 160 μm, indicative of increasing tensile strain. A maximum tensile strain of 1.62% was measured when the pad length was 160 μm; Ge wires with pad lengths greater than 160 μm broke during fabrication. Figure 4b shows that a linear relationship exists between Ge-wire strain and pad length, highlighting excellent Ge-wire lattice-strain controllability. Uniaxial tensile strains as high as 5.7% were achieved in previous work using internal stresses unintentionally applied to GOI substrates. While wires approximately 4.5 μm × 200 nm were used in previous studies [25], 2-μm-wide Ge wire was used in this study; therefore, we conclude that narrower wires facilitate higher strains even by our process without breakage.

Figure 5a shows the photoluminescence (PL) spectra of narrow Ge wires obtained using a micro-PL system at room temperature. Samples were photoexcited by a 647 nm laser beam focused on a sampling spot with a diameter of approximately 1 μm. Light emission was detected from 1.1 to 2.2 μm using a cooled, wavelength-extended InGaAs 1024-pixel linear photodiode array (Princeton Instruments, PyLon-IR-2.2) optically coupled to a spectrograph. We carefully varied the PL measurement conditions, including the excitation laser power and the exposure time. We observed that the PL peak redshifted and became more intense with increasing lattice strain, confirming that Ge-wire bandgap shrinkage is caused by the induced tensile strain. Moreover, the intensity of the PL peak associated with a Ge wire with a 1.62% lattice stain was 30-times higher than that of the Ge substrate.

We next compared the PL peak position with the bandgap energy determined using deformation potential theory, as shown in Figure 5b [28]. While the light- and heavy-hole bands are degenerate in the unstrained Ge crystal, uniaxial tensile strain splits the two bands and positions the light-hole band at a higher energy level than the heavy-hole band. The PL peak position is in good agreement with the bandgap between the heavy-hole band and the conduction band at the Γ point (Γ-HH). The PL spectrum of the Ge wire with a 1.62% tensile strain clearly shows a second peak on the low-energy side, the position of which is consistent with the bandgap between the light-hole band and the conduction band at the Γ point (Γ-LH). The higher PL peak intensity observed for the Γ-HH band gap is ascribable to a higher density of states in the heavy-hole band than in the light-hole band. These results are in good agreement with those obtained for Ge wires fabricated using internal stresses unintentionally applied to GOI substrates [32].

Light-emitting diodes using Ge bridge structures

We fabricated light-emitting diodes (LEDs) using Ge bridge structures bearing uniaxial tensile strains to examine their luminescence properties under current injection. After sputtering W films, phosphorus ion implantation at 2×10^{15} cm^{-2} and activation annealing at 500 °C for 5 min were carried out, followed by wire-and-pad structure patterning, with *p-n* junctions located at the centers of the narrow Ge wires. Finally, Al electrodes were formed on the W and Ge layers. Figure 6a shows the room-temperature voltage-current characteristics of the *p–n* diode with 0.8% tensile strain. We observed good rectifying properties with a 10^4 on/off ratio. Figure 6b shows the electroluminescence (EL) spectra of Ge *p–n* diodes with uniaxial tensile strains of 0, 0.4%, and 0.8%. The clearly evident PL peak was observed to shift to lower energy with increasing tensile strain. The 0.8% strained wire exhibited a peak that was 1.5-times more intense than that of the unstrained wire, confirming that tensile strain enhances optical properties.

Conclusions

We fabricated narrow Ge wires with uniaxial tensile strains by utilizing the internal tensile strains in deposited metal thin films. We found that the strain can be controlled by adjusting the pad length. A maximum strain of 1.62% was recorded for a pad length of 160 μm. The PL peak became more intense and its position shifted to lower energy with increasing tensile strain; the observed peak shifts are in good agreement with theoretical predictions. We also fabricated LEDs using narrow Ge wires and observed clear EL peaks, which demonstrates that the Ge wires exhibit enhanced optical properties.

Acknowledgments

This study was supported by JSPS KAKENHI (grant numbers 20H02620, 21K04880, and 22H01528).

The authors declare that they have no conflicts of interest.

References

[1] D. Thomson, A. Zilkie, J. E. Bowers, T. Komljenovic, G. T. Reed, L. Vivien, D. Marris-Morini, E. Cassan, L. Virot, J-M. Fédéli, J-M. Hartmann, J. H. Schmid, D-X. Xu, F. Boeuf, P. O'Brien, G. Z. Mashanovich, and M. Nedeljkovic, *Roadmap on Silicon Photonics*, J. Opt. **18**, 073003 (2016).

[2] R. Soref, *The Past, Present, and Future of Silicon Photonics*, IEEE J. Sel. Top. Quantum Electron. **12**, 1678 (2006).

[3] B. Jalali and S. Fathpour, *Silicon Photonics*, J. Lightwave Technol. **24**, 4600 (2006).

[4] R. Jones, P. Doussiere, J. B. Driscoll, W. Lin, H. Yu, Y. Akulova, T. Komljenovic, and J. E. Bowers, *Heterogeneously Integrated InP/Silicon Photonics: Fabricating Fully Functional Transceivers*, IEEE Nanotechnol. Mag. **13**, 17 (2019).

[5] J. Michel, J. Liu, and L. C. Kimerling, *High-Performance Ge-on-Si Photodetectors*, Nat. Photonics **4**, 527 (2010).

[6] J. Liu, X. Sun, R. Camacho-Aguilera, L. C. Kimerling, and J. Michel, *Ge-on-Si Laser Operating at Room Temperature*, Opt. Lett. **35**, 679 (2010).

[7] R. E. Camacho-Aguilera, Y. Cai, N. Patel, J. T. Bessette, M. Romagnoli, L. C. Kimerling, and J. Michel, *An Electrically Pumped Germanium Laser*, Opt. Express **20**, 11316 (2012).

[8] S. Gupta, B. Magyari-Köpe, Y. Nishi, and K. C. Saraswat, *Achieving Direct Band Gap in Germanium through Integration of Sn Alloying and External Strain*, J. Appl. Phys. **113**, 073707 (2013).

[9] M. J. Süess, R. Geiger, R. A. Minamisawa, G. Schiefler, J. Frigerio, D. Chrastina, G. Isella, R. Spolenak, J. Faist, and H. Sigg, *Analysis of Enhanced Light Emission from Highly Strained Germanium Microbridges*, Nat. Photonics **7**, 466 (2013).

[10] H. Oka, T. Tomita, T. Hosoi, T. Shimura, and H. Watanabe, *Lightly Doped N-Type Tensile-Strained Single-Crystalline GeSn-on-Insulator Structures Formed by Lateral Liquid-Phase Crystallization*, Appl. Phys. Express **11**, 011304 (2018).

[11] S. Wirths, R. Geiger, N. von den Driesch, G. Mussler, T. Stoica, S. Mantl, Z. Ikonic, M. Luysberg, S. Chiussi, J. M. Hartmann, H. Sigg, J. Faist, D. Buca and D. Grützmacher, *Lasing in Direct-Bandgap GeSn Alloy Grown on Si*, Nat. Photonics **9**, 88 (2015).

[12] A. Elbaz, R. Arefin, E. Sakat, B. Wang, E. Herth, G. Patriarche, A. Foti, R. Ossikovski, S. Sauvage, X. Checoury, K. Pantzas, I. Sagnes, J. Chrétien, L. Casiez, M. Bertrand, V. Calvo, N. Pauc, A. Chelnokov, P. Boucaud, F. Boeuf, V. Reboud, J-M. Hartmann, and M. E. Kurdi, *Reduced Lasing Thresholds in GeSn Microdisk Cavities with Defect Management of the Optically Active Region*, ACS Photonics **7**, 2713 (2020).

[13] V. Reboud, A. Gassenq, N. Pauc, J. Aubin, L. Milord, Q. M. Thai, M. Bertrand, K. Guilloy, D. Rouchon, J. Rothman, T. Zabel, F. A. Pilon, H. Sigg, A. Chelnokov, J. M. Hartmann, and V. Calvo, *Optically Pumped GeSn Micro-Disks with 16% Sn Lasing at 3.1 μ m up to 180 K*, Appl. Phys. Lett. **111**, 092101 (2017).

[14] H. Oka, T. Amamoto, M. Koyama, Y. Imai, S. Kimura, T. Hosoi, T. Shimura, and H. Watanabe, *Fabrication of Tensile-Strained Single-Crystalline GeSn on Transparent Substrate by Nucleation-Controlled Liquid-Phase Crystallization*, Appl. Phys. Lett. **110**, 032104 (2017).

[15] Y. Zhou, W. Dou, W. Du, S. Ojo, H. Tran, S. A. Ghetmiri, J. Liu, G. Sun, R. Soref, J. Margetis, J. Tolle, B. Li, Z. Chen, M. Mortazavi, and S-Q. Yu, *Optically Pumped GeSn Lasers Operating at 270 K with Broad Waveguide Structures on Si*, ACS Photonics **6**, 1434 (2019).

[16] W. Dou, Y. Zhou, J. Margetis, S. A. Ghetmiri, S. Al-Kabi, W. Du, J. Liu, G. Sun, R. A. Soref, J. Tolle, B. Li, M. Mortazavi, and S-Q. Yu, *Optically Pumped Lasing at 3 Mm from Compositionally Graded GeSn with Tin up to 22.3%*, Opt. Lett. **43**, 4558 (2018).

[17] S. Al-Kabi, S. A. Ghetmiri, J. Margetis, T. Pham, Y. Zhou, W. Dou, B. Collier, R. Quinde, W. Du, A. Mosleh, J. Liu, G. Sun, R. A. Soref, J. Tolle, B. Li, M. Mortazavi, H. A. Naseem, and S-Q. Yu, *An Optically Pumped 2.5 μ m GeSn Laser on Si Operating at 110 K*, Appl. Phys. Lett. **109**, 171105 (2016).

[18] H. Oka, T. Tomita, T. Hosoi, T. Shimura, and H. Watanabe, *Lightly Doped N-Type Tensile-Strained Single-Crystalline GeSn-on-Insulator Structures Formed by Lateral Liquid-Phase Crystallization*, Appl. Phys. Express **11**, 011304 (2018).

[19] H. Oka, T. Amamoto, M. Koyama, Y. Imai, S. Kimura, T. Hosoi, T. Shimura, and H. Watanabe, *Fabrication of Tensile-Strained Single-Crystalline GeSn on Transparent Substrate by Nucleation-Controlled Liquid-Phase Crystallization*, Appl. Phys. Lett. **110**, 032104 (2017).

[20] H. Oka, M. Koyama, T. Tomita, T. Amamoto, K. Tominaga, S. Tanaka, T. Hosoi, T. Shimura, and H. Watanabe, *High-Mobility TFT and Enhanced Luminescence Utilizing Nucleation-Controlled GeSn Growth on Transparent Substrate for Monolithic Optoelectronic Integration*, 2016 IEEE International Electron Devices Meeting (IEDM), San Francisco, CA, USA, 2016, pp. 22.1.1-22.1.4.

[21] T. Shimura, M. Matsue, K. Tominaga, K. Kajimura, T. Amamoto, T. Hosoi, and H. Watanabe, *Enhancement of Photoluminescence from N-Type Tensile-Strained GeSn Wires on an Insulator Fabricated by Lateral Liquid-Phase Epitaxy*, Appl. Phys. Lett. **107**, 221109 (2015).

[22] Y. Wada, K. Inoue, T. Hosoi, T. Shimura, and H. Watanabe, *Demonstration of Mm Long Nearly Intrinsic GeSn Single-Crystalline Wires on Quartz Substrate Fabricated by Nucleation-Controlled Liquid-Phase Crystallization*, Jpn. J. Appl. Phys. **58**, SBBK01 (2019).

[23] H. Oka, K. Inoue, T. T. Nguyen, S. Kuroki, T. Hosoi, T. Shimura, and H. Watanabe, *Back-Side Illuminated GeSn Photodiode Array on Quartz Substrate Fabricated by Laser-Induced Liquid-Phase Crystallization for Monolithically-Integrated NIR Imager Chip*, 2017 IEEE International Electron Devices Meeting (IEDM), San Francisco, CA, USA, 2017, pp. 16.3.1-16.3.4.

[24] H. Oka, M. Koyama, T. Hosoi, T. Shimura, and H. Watanabe, *Enhancement-Mode n-Channel TFT and Room-Temperature near-Infrared Emission Based on n^+/p Junction in Single-Crystalline GeSn on Transparent Substrate*, 2017 Symposium on VLSI Technology, Kyoto, Japan, 2017, pp. T58-T59.

[25] D. S. Sukhdeo, D. Nam, J.-H. Kang, M. L. Brongersma, and K. C. Saraswat, *Direct Bandgap Germanium-on-Silicon Inferred from 5.7% (100) Uniaxial Tensile Strain*, Photonics Res. **2**, A8 (2014).

[26] S. Bao, D. Kim, C. Onwukaeme, S. Gupta, K. Saraswat, K. H. Lee, Y. Kim, D. Min, Y. Jung, H. Qiu, H. Wang, E. A. Fitzgerald, C. S. Tan, and D. Nam, *Low-Threshold Optically Pumped Lasing in Highly Strained Germanium Nanowires*, Nat. Commun. **8**, 1845 (2017).

[27] J. Chrétien, N. Pauc, F. A. Pilon, M. Bertrand, Q-M. Thai, L. Casiez, N. Bernier, H. Dansas, P. Gergaud, E. Delamadeleine, R. Khazaka, H. Sigg, J. Faist, A. Chelnokov, V. Reboud, J-M. Hartmann, and V. Calvo, *GeSn Lasers Covering a Wide Wavelength Range Thanks to Uniaxial Tensile Strain*, ACS Photonics **6**, 2462 (2019).

[28] C. G. van de Walle, *Band Lineups and Deformation Potentials in the Model-Solid Theory*, Phys. Rev. B **39**, 1871 (1989).

[29] Y. G. Shen, Y. W. Mai, Q. C. Zhang, D. R. McKenzie, W. D. McFall, and W. E. McBride, *Residual Stress, Microstructure, and Structure of Tungsten Thin Films Deposited by Magnetron Sputtering*, J. Appl. Phys. **87**, 177 (2000).

[30] J. A. Thornton, *Influence of Apparatus Geometry and Deposition Conditions on the Structure and Topography of Thick Sputtered Coatings*, J. Vac. Sci. Technol. **11**, 666 (1974).

[31] G. G. Stoney, *The Tension of Metallic Films Deposited by Electrolysis*, Proc. R. Soc. London, Ser. A **82**, 172 (1909).

[32] D. Nam, D. S. Sukhdeo, S. Gupta, J. H. Kang, M. L. Brongersma, and K. C. Saraswat, *Study of Carrier Statistics in Uniaxially Strained Ge for a Low-Threshold Ge Laser*, IEEE J. Sel. Top. Quantum. Electron. **20**, 16 (2014).

Table I. Sputter deposition conditions of W films with 100 nm thickness.

Base pressure (Pa)	5.0×10^{-4}
Process pressure (Pa)	0.5～4.5
Gas	Ar
Gas flow rate (sccm)	20
Input power (W)	100
Target-sample distance (mm)	80
Deposition time (min)	10

Figure Captions

Fig. 1. Internal stress in W films of 100 nm thickness as a function of Ar gas pressure during deposition.

Fig. 2. Process flow for the fabrication of the Ge bridge with tensile stress induced by W deposition films.

Fig. 3. Schematic drawing and optical images of the Ge bridge structures.

Fig. 4. (a) Raman spectra of narrow Ge wires with pad lengths of 20, 40, 80, 120, and 160 μm. (b) The tensile strain of narrow Ge wires as a function of pad length. The dashed line is a linear fitting result. The strain was estimated using the parameters in ref. [9], showing the relation between Raman shift ($\Delta\omega$) and strain (ε).

Fig. 5. (a) PL spectra of narrow Ge wires with pad lengths of 80, 120, and 160 μm. (b) PL peak positions as a function of uniaxial tensile strain. Solid lines show bandgap energy theoretically estimated using deformation potential energy. Data of the solid lines from reference [32].

Fig. 6. (a) Current-voltage characteristic of the uniaxially tensile-strained Ge *p*-*n* diode. The inset shows the side view of the *p*-*n* diode. (b) Electroluminescence spectra of Ge *p*-*n* diodes with uniaxial tensile strains of 0, 0.4, and 0.8%.

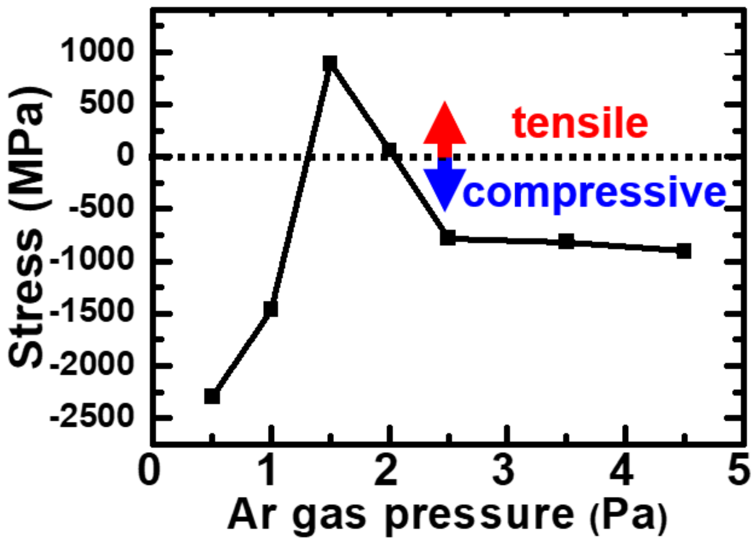
1000
500
0
-500
-1000
-1500
-2000
-2500
Stress (MPa)
tensile
compressive
0
1
2
3
4
5
Ar gas pressure (Pa)

Fig. 1.

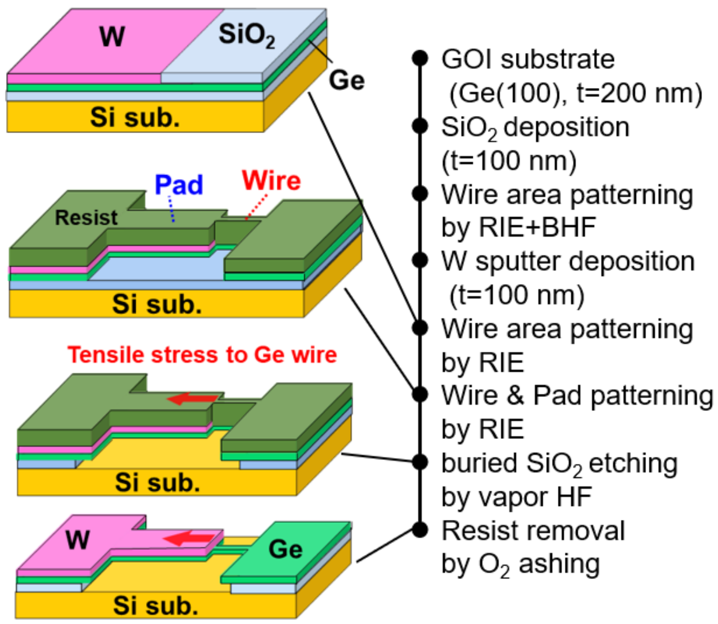
W
SiO_2
Ge
Si sub.
Pad
Wire
Resist
Si sub.
Tensile stress to Ge wire
Si sub.
W
Ge
Si sub.
GOI substrate
(Ge(100), t=200 nm)
SiO_2 deposition
(t=100 nm)
Wire area patterning
by RIE+BHF
W sputter deposition
(t=100 nm)
Wire area patterning
by RIE
Wire & Pad patterning
by RIE
buried SiO_2 etching
by vapor HF
Resist removal
by O_2 ashing

Fig. 2.

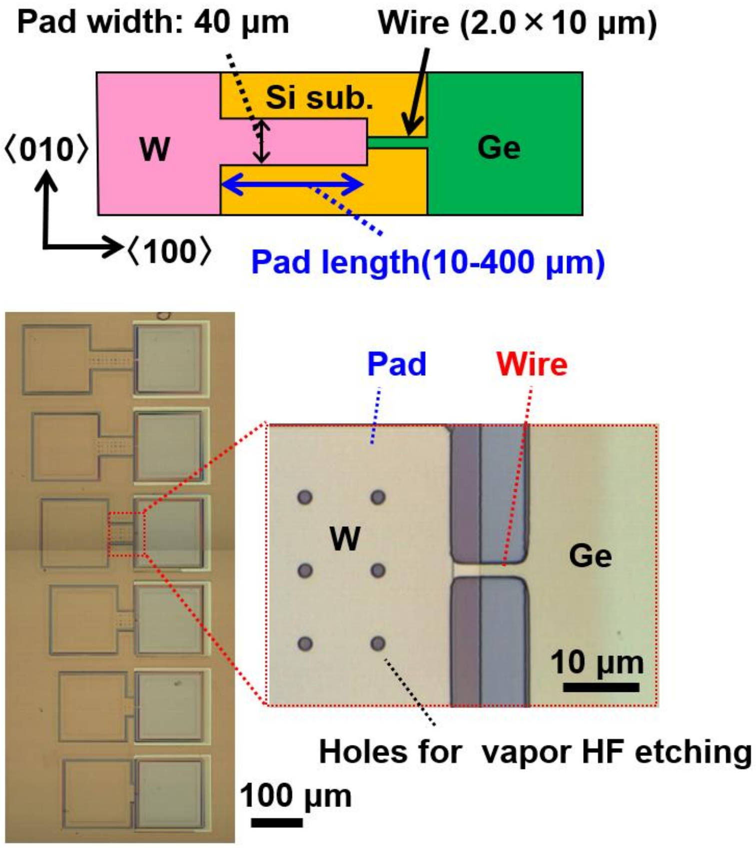
Pad width: 40 μm
Wire (2.0 × 10 μm)
Si sub.
〈010〉
W
Ge
〈100〉
Pad length(10-400 μm)
Pad
Wire
W
Ge
10 μm
Holes for vapor HF etching
100 μm

Fig. 3.

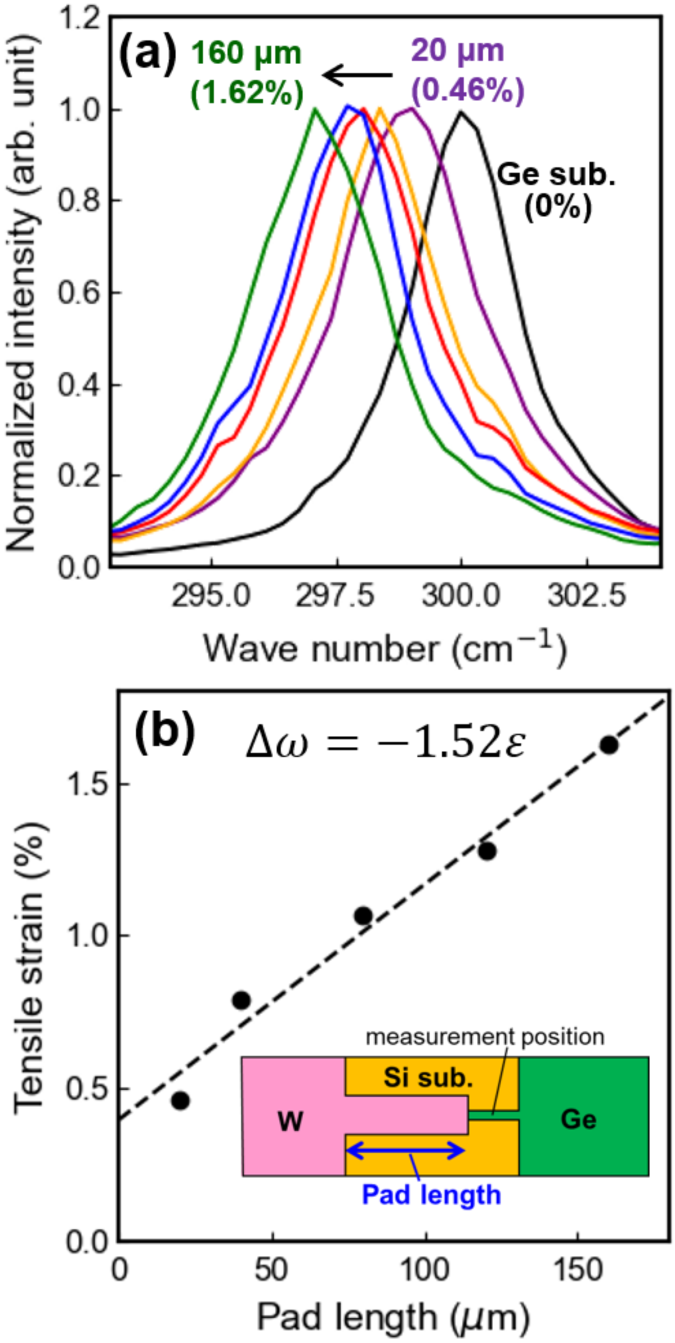
(a)
160 µm
(1.62%)
20 µm
(0.46%)
Ge sub.
(0%)
Normalized intensity (arb. unit)
Wave number (cm^{-1})
(b)
$\Delta\omega = -1.52\varepsilon$
Tensile strain (%)
measurement position
Si sub.
W
Ge
Pad length
Pad length (μm)

Fig. 4.

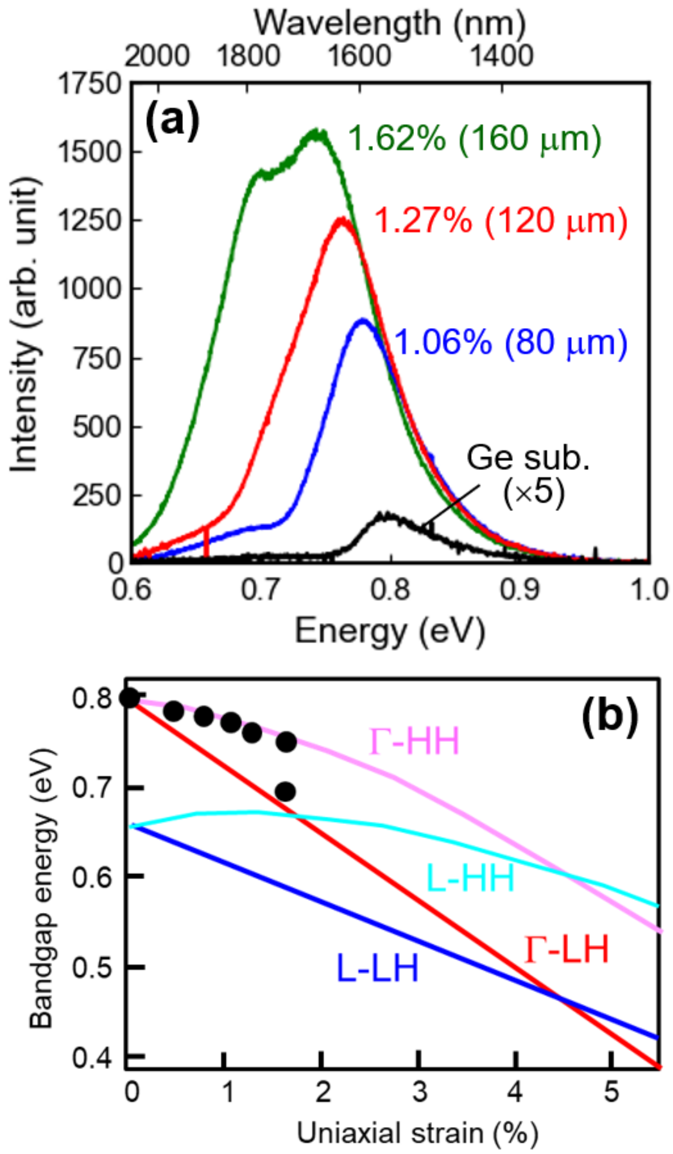
Wavelength (nm)
2000
1800
1600
1400
(a)
1.62% (160 μm)
1.27% (120 μm)
1.06% (80 μm)
Ge sub.
(×5)
Intensity (arb. unit)
1750
1500
1250
1000
750
500
250
0
0.6
0.7
0.8
0.9
1.0
Energy (eV)
(b)
Γ-HH
L-HH
Γ-LH
L-LH
Bandgap energy (eV)
0.8
0.7
0.6
0.5
0.4
0
1
2
3
4
5
Uniaxial strain (%)

Fig. 5.

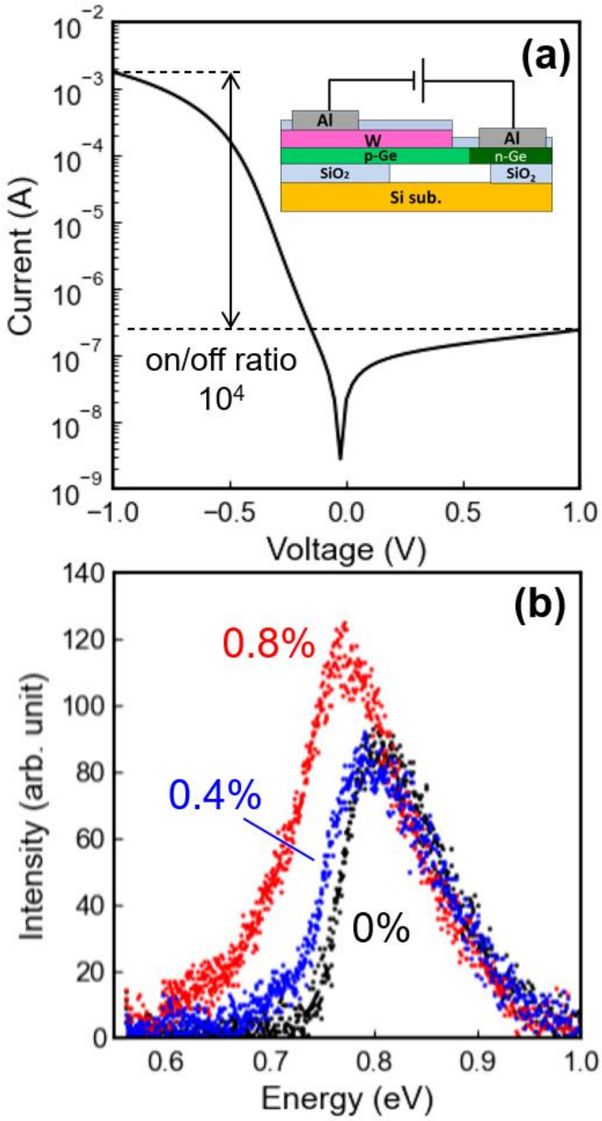
(a)
Al
W
p-Ge
n-Ge
SiO2
SiO2
Si sub.
Current (A)
Voltage (V)
on/off ratio
10^4
(b)
0.8%
0.4%
0%
Intensity (arb. unit)
Energy (eV)

Fig. 6.